Structural and Multidisciplinary Optimization (2025) 68:34
https://doi.org/10.1007/s00158-025-03975-3

RESEARCH PAPER

Minimum size control for binary topology optimization

Rômulo L. Cortez[1] · Mario Setta[2] · Renato Picelli[3] · Eddie Wadbro[2]

Received: 19 August 2024 / Revised: 1 November 2024 / Accepted: 26 January 2025 / Published online: 21 February 2025

Abstract
Topology optimization methods employing binary (also known as discrete) design variables currently lack mathematical formulations to ensure length scale control in their solutions. This paper proposes and applies a morphology-mimicking filtering scheme to provide a minimum size control (often also referred to as minimum length scale control) in this class of binary designs. The Topology Optimization of Binary Structures (TOBS) method was chosen as the foundational framework for this length scale control study. Thermal and structural compliance scenarios were explored under this approach. Numerical results show that the proposed filter efficiently imposes the desired minimum length scale. The optimized designs were also less dependent on the filtering parameters when compared to designs optimized using standard techniques that employ continuous design variables.

Keywords Topology optimization · Binary design variables · Size control · Morphological operators · TOBS method

1 Introduction

Topology optimization (TO) is an advanced computational approach to engineer optimal material distributions in diverse fields such as solid mechanics, acoustics, heat transfer, fluid dynamics, and multiphysics problems (Bendsøe and Sigmund 2003; Wadbro and Berggren 2006; Koga et al. 2013; Picelli et al. 2020a; Yoon and Kim 2005). Ideally, the final designs are binary by nature. That is, the goal is to achieve a configuration where the design variables, often referred to as densities, take a value of '1' to indicate material presence and '0' to signify absence. TO methods that utilize density as design variables are categorized as continuous or binary (also called discrete) methods.

Continuous methods relax the binary constraint to allow intermediate densities between 0 and 1, and a gradient-based method ensures convergence to a local minimum. These methods often require regularization filters or post-processing to achieve nearly binary solutions (Guest 2009; Guest et al. 2011; Huang and Xie 2007; Sigmund 2007). Furthermore, an important class of filters was developed to provide size control of the material regions in the final solution. For instance, the paper by Guest et al. (2004) proposed a method using nodal design variables and projection functions to impose a similar minimum length scale. Lazarov et al. (2016) reviewed advancements in manufacturable designs through density-based topology optimization, focusing on methods to impose minimum and maximum length scales for robust performance. More recently, Hägg and Wadbro (2018) introduced a morphological filter for length scale control that eliminates almost completely the undesirable grayscale and possesses minimum length scales on both phases (solid and void) for minimum compliance problems.

While continuous methods rapidly developed and became popular, binary methods experienced slower-paced development. Although the idea of using binary densities dates back to 1993 (Xie and Steven 1993), some articles reported that integer programming was computationally impractical

Responsible editor: Xu Guo.

Rômulo L. Cortez and Mario Setta have been contributed equally to this work.

✉ Mario Setta
mario.setta@kau.se

[1] Department of Mechanical Engineering, Polytechnic School of the University of São Paulo, Av Prof. Mello Moraes 2231, São Paulo, Brazil

[2] Department of Mathematics and Computer Science, Karlstad University, SE-651 88, Karlstad, Sweden

[3] Department of Naval Architecture and Ocean Engineering, Polytechnic School of the University of São Paulo, Av Prof. Mello Moraes 2231, São Paulo, Brazil

for TO (Beckers 1999; Svanberg and Werne 2006). Fortunately, this is no longer the case (Picelli et al. 2020b). In general, binary methods solve Sequential Approximate Integer Programming (SAIP) problems, in which the objective and constraint functions are linearized. The most popular binary method is the Bi-directional Evolutionary Structural Optimization (BESO), created by Huang and Xie (2007). Although defined by a heuristic design update scheme, the BESO method effectively solves the SAIP problem when only volume constraints are used or when non-volume constraints are shifted to the objective function via Lagrangian multipliers (Xu et al. 2023). More recently, two similar SAIP-based formulations were proposed to allow the binary methods to directly include multiple non-volume constraints in the SAIP problem. Sivapuram and Picelli (2018) proposed the Topology Optimization of Binary Structures (TOBS) method by formulating a SAIP problem and solving it with the branch-and-bound algorithm. Meanwhile, Liang and Cheng (2019) used the Canonical Dual Theory (CDT) to solve the SAIP problem and reformulated the method with a trust region procedure (Liang and Cheng 2020). Today, binary methods are an alternative for a range of different academic problems (Xia et al. 2018; Sun et al. 2024), including promising 3D designs (Lai et al. 2024), and recent advancements have also explored the feasibility of implementing binary design variables at node-wise variables in turbulent flow optimization (Alonso et al. 2022).

Compared to continuous methods, binary methods lag in ensuring length scale control of their solutions. In fact, to the best of the authors' knowledge, only a limited number of studies, notably two, have ventured into attempting to control the length scale. Qiu et al. (2022), using the BESO method, introduced a p-norm constraint to consolidate a local maximum length scale control. Zhao et al. (2018) devised a maximum length scale control scheme tailored for the internal structural design of emergent plants, inspired by the intricate internal textures of leaf veins and grass. These methods introduce additional constraints to the problem, rendering it computationally challenging and less scalable. Furthermore, they do not mathematically guarantee the simultaneous length scale control of both solid and void regions.

In this paper, we present an approach to ensure minimum length scale control in binary topology optimization using morphological operators as a filtering technique. This method achieves its goals without parameter continuation or new constraints and offers a mathematical guarantee of length scale control in binary topology optimization. We chose the TOBS method due to its robustness and formal mathematical programming basis. Our proposed morphological filter is versatile and adaptable to a broader range of binary topology optimization and SAIP models, enhancing its practicality.

The current length scale control formulation is similar to the one previously employed by Hägg and Wadbro (2018) in a continuous method framework. In the present approach, the formulation guarantees binary (0/1) outcomes and appears less dependent on parameter tuning. It also ensures clarity in the final design and possibly enhances manufacturability. The minimal requirement for parameter tuning, coupled with its inherent stability and rapid convergence of the SAIP problem, significantly enhances user-friendliness and computational efficiency. The method's general applicability across different optimization scenarios and its straightforward implementation protocol further underscore its utility.

2 Problem statement

The most popular topology optimization problem is the minimum compliance design. This type of problem is widely used to compare proposed methodologies. In this paper, all optimization problems can be described as:

$$\begin{aligned} &\min_{\mathbf{x}} c(\mathbf{x}), \\ &\text{s.t. } v(\mathbf{x}) \le \overline{V}, \\ &\quad x_j \in \{0,1\},\ j = 1,\dots,N_d. \end{aligned} \tag{1}$$

Here, the decision variables $\mathbf{x}$ encode the design, as further detailed in Sect. 3, $c(\mathbf{x})$ is the (structural or thermal) compliance, $v(\mathbf{x})$ is a measure of the volume of the design, and $\overline{V}$ is a bound on the volume. For the numerical experiments presented in this paper, $\overline{V}$ is fixed to 50% of the size of the design domain.

2.1 Thermal compliance

The thermal compliance problem focuses on optimizing the material distribution within a given design domain to minimize thermal compliance. Figure 1 shows the design domain Ω for this problem. In this setup, the domain is subject to a uniform heating force q, the boundary segment Γ_D maintains the temperature at zero, while the remainder of the boundary, Γ_N, is insulated. That is, the temperature t satisfies

$$\begin{aligned} -\nabla\cdot(\kappa(\mathbf{x})\nabla t) &= q \quad \text{in } \Omega, \\ t &= 0 \quad \text{on } \Gamma_D, \\ \frac{\partial t}{\partial n} &= 0 \quad \text{on } \Gamma_N, \end{aligned} \tag{2}$$

where n denotes the outward directed normal and $\kappa(\mathbf{x})$ is the conductivity, which depends on the current design.

The goal of the thermal compliance problem in topology optimization is to minimize the average temperature at thermal equilibrium, subject to a volume constraint. The problem can be formulated as follows. We discretize the domain Ω into

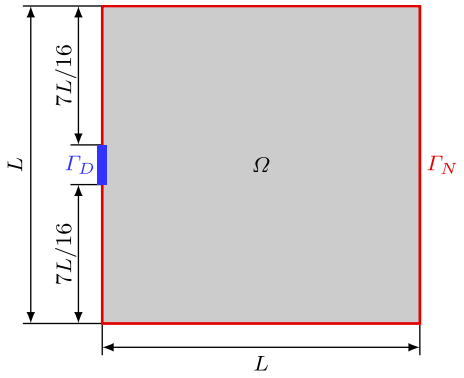

Fig. 1 Schematic representation of the heat problem domain and its boundaries

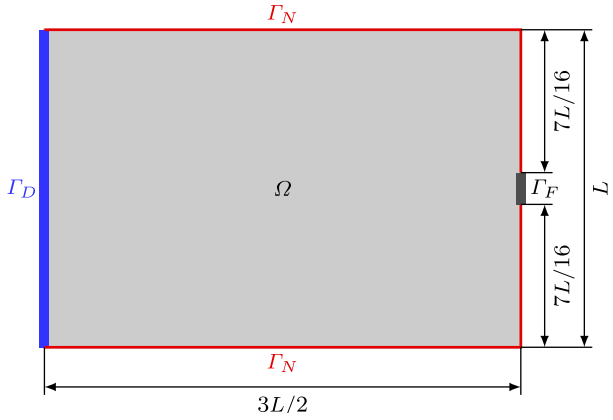

Fig. 2 Schematic representation of the domain for the cantilever beam problem and its boundaries

square elements and use bi-linear finite elements to numerically solve the governing equation. After discretization, the governing equation for steady-state heat distribution is

$$\mathbf{K}_{\mathrm{t}}(\mathbf{x})\mathbf{t} = \mathbf{q}, \tag{3}$$

where $\mathbf{t}$ holds the nodal values of the temperature, and the stiffness matrix $\mathbf{K}_{\mathrm{t}}$ and the right-hand side vector $\mathbf{q}$ have entries

$$\begin{aligned} k_{ij} &= \int_{\Omega} \kappa \nabla\varphi_i \cdot \nabla\varphi_j, \\ q_i &= \int_{\Omega} q\varphi_i, \end{aligned} \tag{4}$$

respectively. Here, φ_i, $i \in \{1, \ldots, n\}$ are the finite element basis functions. The thermal compliance is given as

$$c_{\mathrm{thermal}} = \mathbf{q}^T\mathbf{t}. \tag{5}$$

2.2 Structural compliance

As our second test case, we consider the problem of minimizing the structural compliance of a cantilever beam. Figure 2 illustrates the design domain Ω and identifies the boundaries where the boundary conditions are applied. The cantilever beam is fixed on its left side and subjected to a uniformly distributed vertical load on a specified portion, Γ_F, on the right side. Assuming we are in the linearly elastic regime, the equilibrium displacement u satisfies

$$\begin{aligned} -\nabla \cdot (E(\mathbf{x})\epsilon(u)) &= 0 \quad \text{in } \Omega, \\ u &= 0 \quad \text{on } \Gamma_D, \\ E(\mathbf{x})\epsilon(u) \cdot n &= 0 \quad \text{on } \Gamma_N, \\ E(\mathbf{x})\epsilon(u) \cdot n &= f \quad \text{on } \Gamma_F, \end{aligned} \tag{6}$$

where n denotes the outward directed normal, $\epsilon(u) = (\nabla u + \nabla u^T)/2$ is the symmetric second order strain tensor, and $E(\mathbf{x})$ is the fourth order elasticity tensor, which depends on the current design. The objective of the structural compliance problem is to find the optimal material distribution within a design domain that minimizes the structure's compliance, ensuring maximum stiffness.

We discretize the domain Ω into square elements and use bi-linear vector-valued finite elements to numerically solve the governing equation. After discretization, the governing equation is

$$\mathbf{K}_{\mathrm{s}}(\mathbf{x})\mathbf{u} = \mathbf{f}, \tag{7}$$

where $\mathbf{u}$ holds the nodal values of the displacement, and the stiffness matrix $\mathbf{K}_{\mathrm{s}}$ and the right-hand side vector $\mathbf{f}$ have entries

$$\begin{aligned} k_{ij} &= \int_{\Omega} E\epsilon(\varphi_i) : \epsilon(\varphi_j), \\ f_i &= \int_{\Gamma_f} f \cdot \varphi_i, \end{aligned} \tag{8}$$

respectively. Here, φ_i, $i \in \{1, \ldots, n\}$ are the finite element basis functions. The compliance of a structure is defined as the work done by external forces. In our case, the compliance can be expressed as:

$$c_{\mathrm{structural}} = \mathbf{f}^T\mathbf{u}. \tag{9}$$

3 Design encoding

Consider a design optimization problem defined on a subset $\Omega \in \mathbb{R}^n$. We describe the design using a binary material distribution function

$$x : \Omega \longrightarrow \{0, 1\}. \tag{10}$$

In the most basic setting, $x = 1$ represents the presence of material, while $x = 0$ represents absence. It is important to note that the binary minimal compliance problem is ill-posed in its basic form. In the following sections, we elaborate on the regularization method employed in our current work and explain how the binary material distribution function relates to the conductivity and the elasticity tensor for the thermal and structural compliance problem, respectively.

Here, we discretize the design domain Ω into N_d elements, $\Omega_1, \ldots, \Omega_{N_d}$. We discretize the material distribution function to be elementwise constant. Thus, we express the design as the vector $\mathbf{x} \in \{0, 1\}^{N_d}$, where x_i holds the value corresponding to element Ω_i, $i = 1, \ldots, N_d$.

Adopting a discrete binary design allows us to use mathematical morphology. Mathematical morphology (Matheron and Serra 2001) explores the geometric properties of a binary image by investigating it with a smaller set called a structuring element. In this context, the structuring element $S_r(\Omega_i)$ is a ball with radius r centered in the element Ω_i. We define $\mathcal{N}_i$ to be the set of indices of the elements in the neighborhood of Ω_i; that is, $j \in \mathcal{N}_i$ if the center of Ω_j is in $S_r(\Omega_i)$.

The erode and dilate operators are two fundamental morphological operators. Intuitively, the erode operator trims a strip from the border of the design. The width of this strip is determined by the structuring element's radius. Conversely, the dilate operator adds material in a strip along the design's boundary. Consequently, the dilate operator fills any void in the design that is smaller than the operator's diameter. Formally, we can define them as min and max operators, respectively (Hägg and Wadbro 2018). Using $\mathcal{N}_i$, we define the erode and dilate operators of the design $\mathbf{x}$ in Ω_i as

$$\mathcal{E}_\Omega(\mathbf{x})_i = \min_{j \in \mathcal{N}_i} x_j \tag{11}$$

and

$$\mathcal{D}_\Omega(\mathbf{x})_i = \max_{j \in \mathcal{N}_i} x_j, \tag{12}$$

respectively. Moreover, by combining the erode and the dilate operator, we obtain the open and the close operators as

$$\mathcal{O}_\Omega(\mathbf{x}) = \mathcal{D}_\Omega(\mathcal{E}_\Omega(\mathbf{x})) \tag{13}$$

and

$$\mathcal{C}_\Omega(\mathbf{x}) = \mathcal{E}_\Omega(\mathcal{D}_\Omega(\mathbf{x})), \tag{14}$$

respectively. Figure 3 demonstrates the effects of the erode (iii), the dilate (iv), the open (v), and the close (vi) operators applied to the test design (ii). The structuring element S_r (i) gives the operators' radius. It is worth noting that the dilate and the close operators are filling any void features smaller than the operators' diameter. This behavior stems directly from the definitions above.

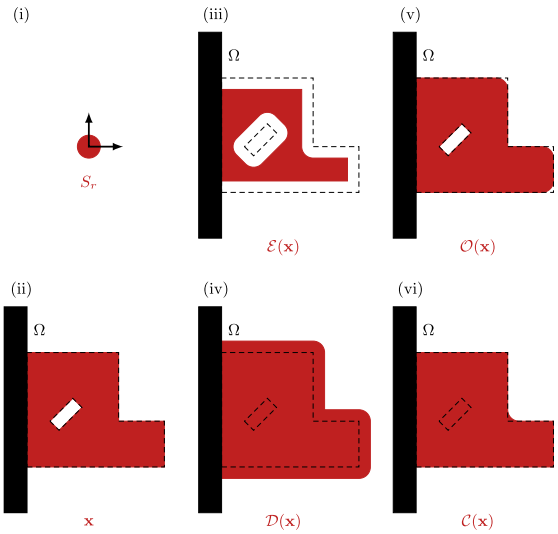

Fig. 3 Illustration of the effects of the morphological operators applied to a binary test design (ii). The radius r of the ball S_r in (i) indicates the radius of the operators. In order, we show the erode (iii), the dilate (iv), the open (v), and the close (vi) morphological operators

We note that the definitions of the morphological operators above only use information on the material indicator on Ω. To avoid boundary effects arising from that Ω is bounded, we use an extended domain approach. That is, we extend the domain to $\tilde{\Omega}$ by padding the boundary of Ω with a rectangular strip of thickness greater than r. Moreover, we discretize the extended domain $\tilde{\Omega}$ into $N_s > N_d$ elements, $\tilde{\Omega}_1, \ldots, \tilde{\Omega}_{N_s}$, where the first N_d elements discretize Ω. Similarly, we extend the discrete material distribution function $\mathbf{x}$ to $\tilde{\mathbf{x}}$ such that $\tilde{\mathbf{x}} \in \{0, 1\}^{N_s}$, such that $\tilde{x}_i = x_i$ for $i = 1, \ldots, N_d$ and $\tilde{x}_i = 0$ for all $i > N_d$.

To employ an optimization method that utilizes gradient information, we cannot use the morphological operators defined above. Thus, we adopt *fW*-mean filters as a continuous approximation of morphological operators (Wadbro and Hägg 2015). Specifically, we consider harmonic filters (Svanberg and Svärd 2013). So, we define the harmonic erode filter on the extended domain as

$$\mathcal{E}^\alpha_{\tilde{\Omega}}(\tilde{\mathbf{x}}) = f_\alpha^{-1}(\boldsymbol{W} f_\alpha(\tilde{\mathbf{x}})), \tag{15}$$

where the functions f_α and f_α^{-1} are applied entrywise. Here,

$$f_\alpha(x) = \frac{1}{x + \alpha} \tag{16}$$

and f_α^{-1} is its inverse, with $\alpha > 0$ being a non-linearity parameter. The harmonic filters converge to their morphological

operator counterparts for $\alpha \to 0$. Here, the weight matrix $\boldsymbol{W} \in \mathbb{R}^{N_s \times N_s}$ has entries

$$w_{ij} = \begin{cases} |\tilde{\mathcal{N}}_i|^{-1} & \text{if } j \in \tilde{\mathcal{N}}_i, \\ 0 & \text{if } j \notin \tilde{\mathcal{N}}_i, \end{cases} \tag{17}$$

where $\tilde{\mathcal{N}}_i$ is the neighborhood of $\tilde{\Omega}_i$ in $\tilde{\Omega}$ and $|\tilde{\mathcal{N}}_i|$ its cardinality. We define the harmonic dilate filter as

$$\mathcal{D}^{\alpha}_{\tilde{\Omega}}(\tilde{\mathbf{x}}) = \mathbf{1} - \mathcal{E}^{\alpha}(\mathbf{1} - \tilde{\mathbf{x}}), \tag{18}$$

where $\mathbf{1} = (1, \dots, 1)^T \in \mathbb{R}^{N_s}$. Finally, the harmonic open and the harmonic close are

$$\mathcal{O}^{\alpha}_{\Omega}(\mathbf{x}) = \mathcal{D}^{\alpha}_{\tilde{\Omega}}(\mathcal{E}^{\alpha}_{\tilde{\Omega}}(\tilde{\mathbf{x}}))|_{\Omega} \tag{19}$$

and

$$\mathcal{C}^{\alpha}_{\Omega}(\mathbf{x}) = \mathcal{E}^{\alpha}_{\tilde{\Omega}}(\mathcal{D}^{\alpha}_{\tilde{\Omega}}(\tilde{\mathbf{x}}))|_{\Omega}, \tag{20}$$

respectively. In other words, we first extend the design $\mathbf{x}$ to $\tilde{\Omega}$ to perform the erosion and dilation operations, respectively, and then restrict the result to Ω.

In the context of minimum compliance problems, to achieve length scale control we adopt the heuristic approach proposed by Hägg and Wadbro (2018), which relies on NEighborhood-based minimum Length scale (NEL) properties of both material and void regions. The strategy is to use the open-filtered design and a SIMP interpolation when evaluating the compliance while using the close-filtered design in the volume constraint. The rationale behind this approach stems from the relation between the open and close morphological operator, namely,

$$(\mathcal{O}_{\Omega}(\mathbf{x}))^p \le \mathcal{O}_{\Omega}(\mathbf{x}) \le \mathbf{x} \le \mathcal{C}_{\Omega}(\mathbf{x}). \tag{21}$$

Remark 1 For vector inequalities, such as those above, $\boldsymbol{a} \le \boldsymbol{b}$ means that all entries of $\boldsymbol{a}$ are smaller than their counterpart in $\boldsymbol{b}$. That is, $\boldsymbol{a} \le \boldsymbol{b}$ if and only if $a_j \le b_j$ for all j.

The idea is that the elements Ω_i where $(\mathcal{O}_{\Omega}(\mathbf{x}))^p < \mathcal{C}_{\Omega}(\mathbf{x})$ have more cost in the constraints and less contribution in the governing equation. Therefore, this strategy promotes designs satisfying $\mathcal{O}^p_{\Omega}(\mathbf{x}) = \mathcal{C}_{\Omega}(\mathbf{x})$. That is designs with minimum length scale control on both the structural and the void region.

More specifically, the relative volume is

$$v(\boldsymbol{x}) = \frac{1}{N_d} \sum_{j=1}^{N_d} \mathcal{C}^{\alpha}_{\Omega}(\mathbf{x})_j.$$

Moreover, $j = 1, \dots, N_d$, we define the physical density in Ω_j by

$$P(\boldsymbol{x})_j = \underline{\rho} + (1 - \underline{\rho})(\mathcal{O}^{\alpha}_{\Omega}(x))^p_j, \tag{22}$$

where $\underline{\rho} > 0$ is a minimum physical density and $p \ge 1$ is the SIMP penalty parameter. Utilizing the physical density, we define the conductivity and elasticity tensor that enters the governing equations by $\kappa(\boldsymbol{x}) = P(\boldsymbol{x})$ and $E(\boldsymbol{x}) = P(\boldsymbol{x})E_0$, where E_0 is the elasticity tensor of the base material, respectively. We use these quantities when solving the governing equations (3) and (7) and then we evaluate the corresponding compliances according to equations (5) and (9), respectively.

To examine the difference between the open and close filters, we use the following quality measure (Hägg and Wadbro 2018):

$$F_{\text{DOC}} = \frac{\text{card}\{i \mid (\mathcal{C}^{\alpha}_{\Omega}(\mathbf{x}) - \mathcal{O}^{\alpha}_{\Omega}(\mathbf{x}))_i > 0.5\}}{N_d}. \tag{23}$$

This represents the fraction of elements where the difference between $\mathcal{O}^{\alpha}_{\Omega}(\mathbf{x})$ and $\mathcal{C}^{\alpha}_{\Omega}(\mathbf{x})$ is greater than a cutoff value of 0.5.

The use of *fW*-mean filters in this approach allows for gradient-based topology optimization methods. Nonetheless, we still need a way to compute the sensitivities of the objective and constraint functions with respect to the design variables x_i. We calculate the gradient of the objective and constraint functions applying the chain rule on the specific filter sequence relative to the open and close filters, respectively. For more details, as well as code snippets detailing this procedure, we refer the reader to Sections 4.2-−4.4 in the article by Hägg and Wadbro (2017).

4 The TOBS method

The TOBS method has emerged as a well-documented and applied approach in the field of structural optimization, particularly in the class of binary methods. This methodology formulates a SAIP-based problem and ensures that the final optimized structures are strictly binary, consisting exclusively of solid material or void, thereby directly eliminating the existence of intermediate-density elements.

Consider a generic topology optimization problem on a physical system:

$$\begin{aligned} &\underset{\mathbf{x}}{\text{Minimize}}\, f(\mathbf{x}) \\ &\text{Subject to governing equations} \\ &\qquad g_i(\mathbf{x}) \le \overline{g}_i, \quad i = 1, \dots, N_g, \\ &\qquad \mathbf{x}_j \in \{0, 1\}, \quad j = 1, \dots, N_d, \end{aligned} \tag{24}$$

where $f(\mathbf{x})$ is the objective function, and $g_i(\mathbf{x}) \le \overline{g}_i$ are N_g constraints. The TOBS method employs linearization of problem (24) to transform the non-linear optimization

problem into a linear form suitable for integer linear programming (ILP). This process involves approximating the non-linear relationships using Taylor's series expansion and truncating the series at the linear part. The objective function, for instance, is typically represented in a linearized form as follows:

$$f(\mathbf{x}) \approx f(\mathbf{x}^k) + \frac{\partial f(\mathbf{x}^k)}{\partial \mathbf{x}} \cdot \Delta \mathbf{x}^k. \tag{25}$$

Here, $\mathbf{x}^k$ is the design at iteration k and $\Delta \mathbf{x}^k$ indicates the changes in the design variables within the linearized subproblem. If an element is initially solid ($x_j^k = 1$), Δx_j^k can take on the values of -1 or 0, representing the element's potential transition to void or the maintenance of the solid state. Conversely, for an element that is void ($x_j^k = 0$), Δx_j^k may assume the values of 1 or 0, indicating a shift to solid or the maintenance of the void state. This is expressed as:

$$\Delta x_j^k \in \begin{cases} \{0, 1\} & \text{if } x_j^k = 0, \\ \{-1, 0\} & \text{if } x_j^k = 1, \end{cases}$$

or, in a unified form,

$$\Delta x_j^k \in \{-x_j^k, 1 - x_j^k\}.$$

Linearizing the objective and constraints is crucial for converting the non-linear structural optimization problem into a formulation amenable to ILP solvers. A key feature of the TOBS method is the management of material distribution shifts across iterations, controlled by the flip limit parameter β, which constrains the number of elements that can transition from solid to void and from void to solid in each iteration. Mathematically, this constraint can be expressed as

$$\left\| \Delta \mathbf{x}^k \right\|_1 \leq \beta N_d. \tag{26}$$

The parameter β is crucial for ensuring stability in the optimization process and avoiding drastic changes in the design from one iteration to the next, thus contributing to the convergence and robustness of the TOBS methodology. Thus, the SAIP problem is formulated as:

$$\begin{aligned} &\min_{\Delta \mathbf{x}^k} \ \frac{\partial f(\mathbf{x}^k)}{\partial \mathbf{x}} \cdot \Delta \mathbf{x}^k, \\ &\text{s.t.} \ \frac{\partial g_i(\mathbf{x}^k)}{\partial \mathbf{x}} \cdot \Delta \mathbf{x}^k \leq \Delta g_i^k, \ \ i = 1, \ldots, N_g, \\ &\quad \left\| \Delta \mathbf{x}^k \right\|_1 \leq \beta N_d, \\ &\quad \Delta x_j^k \in \{-x_j^k, 1 - x_j^k\}, \ \ j = 1, \ldots, N_d. \end{aligned} \tag{27}$$

To accommodate potential infeasibility while still allowing for significant topological changes, the TOBS method involves the relaxation of constraints limiting the change in the constraint value to Δg_i^k. This relaxation, as stated in Equation (28) below, generates subproblems that invariably produce feasible solutions, even when initiated from a non-viable initial design. This flexibility proves particularly beneficial when the optimizer is initialized far from the feasible domain, such as starting with a fully solid design domain coupled with a strict volume constraint. The modified constraint bounds are expressed through the relaxation parameter, ϵ, and are mathematically articulated as:

$$\Delta g_i^k = \begin{cases} -\epsilon_i g_i(\mathbf{x}^k) & \text{if } \overline{g}_i < (1 - \epsilon_i) g_i(\mathbf{x}^k), \\ \epsilon_i g_i(\mathbf{x}^k) & \text{if } \overline{g}_i > (1 + \epsilon_i) g_i(\mathbf{x}^k), \\ \overline{g}_i - g_i(\mathbf{x}^k) & \text{otherwise}, \end{cases} \tag{28}$$

where ϵ_i is the relaxation parameter corresponding to each constraint g_i.

The filtering process is the final crucial ingredient of the TOBS methodology, serving to mitigate issues associated with the emergence of checkerboard patterns, which are common in topology optimization. By integrating the proposed method, we ensure that these common pitfalls are addressed, thereby improving the solution quality. Moreover, the filtering technique is carefully calibrated to control the minimum length scale, further enhancing the structural integrity and manufacturability of the optimized design.

5 Numerical experiments and discussion

This section presents the results of employing the TOBS method for minimum length scale control, demonstrated through two distinct examples. All computational tests were executed using MATLAB R2019a on a system powered by a 12th Generation Intel® Core™ i5-12400, clocked at 2.50 GHz, and supported by 16GB of RAM.

For the context of these results, where not otherwise specified, the parameters are set as follows: the non-linearity parameter $\alpha = 10^{-8}$, the TOBS constraint relaxation, $\epsilon = 0.01$, flip limits parameter $\beta = 0.05$, the SIMP penalization is $p = 3$ and the minimum physical density held at $\rho_0 = 10^{-3}$.

We use a reference solution to compare the final optimized designs. The reference solution is computed by solving the variable thickness sheet problem, which is the minimum compliance problem allowing intermediate design variables without any filtering or penalization. The variable thickness problem is convex, allowing us to solve it to global optimality. Thus, we compare the compliance of the TOBS-optimized designs with that of the optimal variable thickness sheet solution. This comparison provides a benchmark for evaluating the effectiveness of the present method by illustrating how closely the optimized designs approach the best possible solution.

5.1 Minimum thermal compliance

This section presents our initial investigation, which focuses on the thermal compliance problem, where the objective is to minimize thermal compliance on a uniformly heated square plate. The structural domain, of side L, is uniformly divided into $n = n_x^2$ square elements.

The entire domain is simulated with Equation (3). Due to the symmetric nature of the problem's geometry, only the top half of the domain was subjected to integer programming optimization, i.e., the number of design variables is half of the total number of finite elements. The topology results from the top half are mirrored onto the bottom half in the resulting figures, providing a complete representation of the entire domain. This approach, suggested by Picelli et al. (2020b), ensures symmetry in binary topology optimization.

In this study, we examine the effects of selected key parameters on the topology optimization procedure, with a particular emphasis on the filter radius, r, and the non-linearity parameter, α. The outcomes of this study, considering different values of r, are illustrated in Fig. 4.

We present various designs demonstrating the effectiveness of the minimum length control method in optimizing the structure while adhering to size constraints. Adjacent to each final design, a red "circle" depicts the neighborhood used in the filtering, visually representing the parameter's

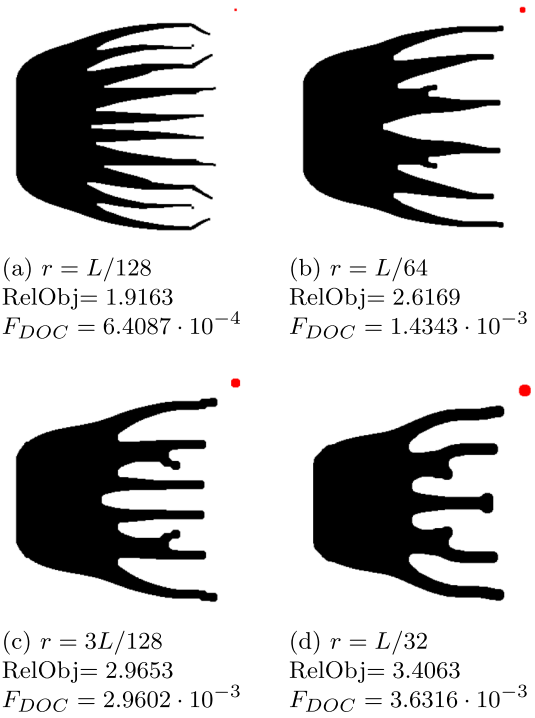

(a) $r = L/128$
RelObj= 1.9163
$F_{DOC} = 6.4087 \cdot 10^{-4}$

(b) $r = L/64$
RelObj= 2.6169
$F_{DOC} = 1.4343 \cdot 10^{-3}$

(c) $r = 3L/128$
RelObj= 2.9653
$F_{DOC} = 2.9602 \cdot 10^{-3}$

(d) $r = L/32$
RelObj= 3.4063
$F_{DOC} = 3.6316 \cdot 10^{-3}$

Fig. 4 Optimized designs for minimal thermal compliance for varying filter radii r. The red region next to each design depicts the used filter kernel's shape and size

influence on the results. Moreover, the value of RelObj below each optimized design indicates the corresponding relative objective function value, which is obtained by dividing the optimized design's compliance c_{thermal} by the compliance of the solution of the variable thickness sheet problem.

The designs in Fig. 4 show the comparative efficacy and resultant configurations with varying r parameters. For a smaller filter radius of $r = L/128$, the optimized design exhibits finer features with multiple narrow bars and structural branches.

As the filter radius increases to $r = L/64$ and $r = 3L/128$, we observe a clear transition toward smoother and more cohesive structures. The optimized designs appear more consolidated, with fewer isolated features. The role of the filter in controlling the minimum feature size becomes more pronounced. For instance, at $r = L/64$, the optimization appears to have limited the smallest structural branches to a span of roughly eight elements, which is the filters' diameter—the results were computed on a 256×256 mesh. This showcases the filter's capability to temper and control the minimum feature size, ensuring an equilibrium between design precision and structural robustness.

For a filter radius of $r = L/32$, the corresponding optimized design appears significantly more streamlined, with broader structural bars. This larger filter has effectively regularized the design space, eliminating smaller features, and leading to an optimized structure. However, this also indicates a potential trade-off: while the larger filter ensures a more robust and connected design, it might sacrifice local design intricacies that could be crucial to minimizing the objective function.

Moreover, the order of magnitude of the F_{DOC} values is between 10^{-4} and 10^{-3}. The latter indicates that the fraction of elements where the open and the close-filtered designs are significantly different is low, confirming that the final designs achieve minimum length scale control.

Figure 5 provides a clear view of how compliance changes throughout the optimization process for different filter radii. For the smallest filter radius, $r = L/128$, we obtain the lowest final compliance for the given volume constraint. This suggests that the optimizer can capture more design details with a smaller filter, but this might lead to thinner structures and possibly be prone to mechanical failure. As the filter size increases, the designs become more regular and less noisy. However, they might not always achieve the best possible compliance, especially when compared to designs with a smaller filter radius.

In this thermal compliance minimization problem, an overall increase in compliance over iterations may be observed. This counterintuitive behavior can be explained by considering the initial design state. The starting design is fully solid, so the volume constraint is not satisfied. As the optimizer progresses, it removes material to meet the

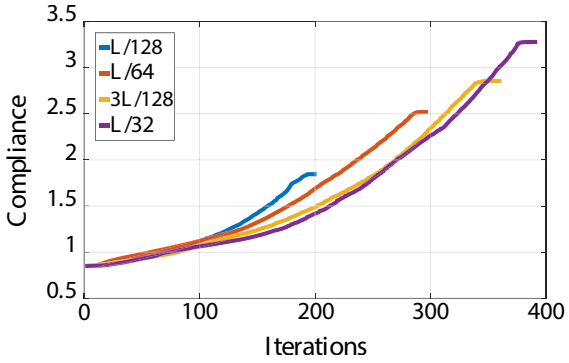

Fig. 5 Variation in the compliance evolution using different filter radii, highlighting the trade-offs between design precision and resulting compliance

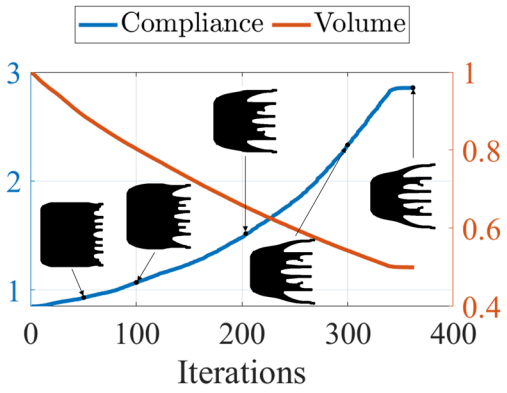

Fig. 6 Compliance vs volume fraction evolution for the design optimized with filter radius $r = 3L/128$. The thumbnails show snapshots of the design's evolution at the marked iterations

prescribed volume constraint. Figure 6 illustrates the evolution of the geometry during the optimization process, capturing various stages of material removal and distribution. These snapshots depict the transformation from the initial full-material state to the final optimized topology. Consequently, as the material is reduced, the thermal compliance value tends to increase due to diminished conductivity in the design. Ultimately, we achieve an optimized 0/1 distribution adapted to the prescribed volume.

Figure 7 presents four distinct optimized designs, each corresponding to different filter radii, r, of $L/128$, $L/64$, $3L/128$, and $L/32$, and initiated from a topology with a central circular void region. The aim is to observe the topological alterations through iterative optimization stages.

Despite the inclusion of elements within the initial void region in the optimization process, the optimizer does not populate this area as might be expected. The reason for this phenomenon lies in the characteristics of the SIMP interpolation used in this study. The sensitivity in the void region is effectively zero due to the choice of using SIMP,

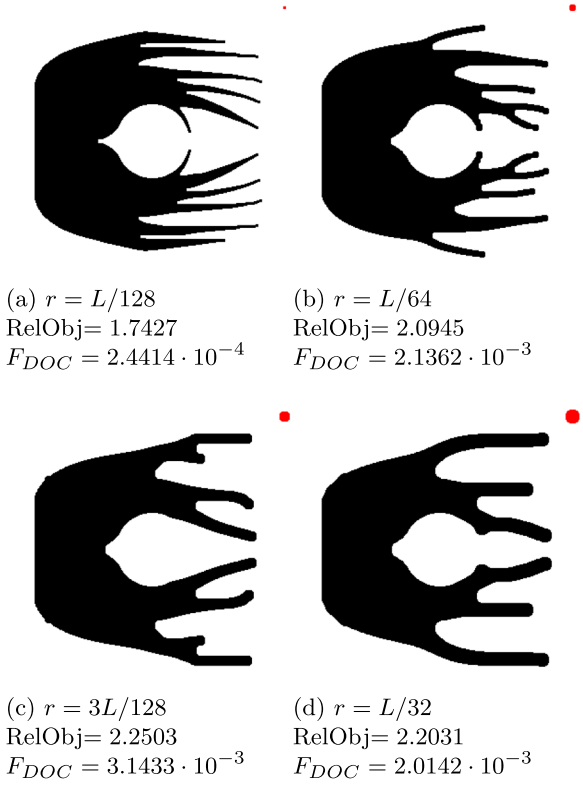

Fig. 7 Final designs for the thermal compliance problem using an alternative initial guess, where the center ball of the design region is void for various filter radii r. The red region next to each design depicts the used filter kernel's shape and size

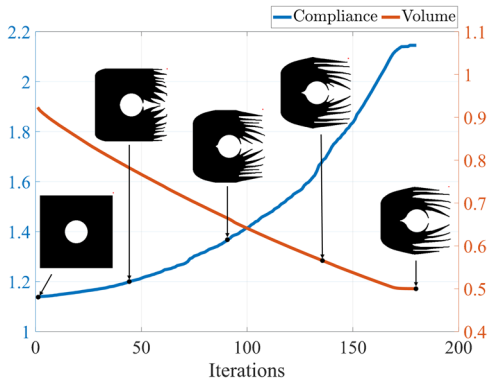

Fig. 8 Compliance vs constraint history for the center ball case optimized with filter radius $r = L/128$. The thumbnails show snapshots of the design's evolution at the marked iterations

resulting in sparse element placement within it throughout the optimization.

Figure 8 displays the evolution of the design in Fig. 7a and its compliance during the optimization process. Here, we show various stages of material removal and distribution from the initial full-material state to the final optimized

geometry. Consequently, as the material is reduced, the thermal compliance value tends to increase due to diminished conductivity in the design. Ultimately, we achieve an optimized 0/1 distribution adapted to the prescribed volume.

Figure 9 displays four distinct topology optimization results, each corresponding to a different value of the non-linearity parameter α, specifically $10^{-4}, 10^{-6}, 10^{-8}$, and 10^{-10}, all with a radius constraint $r = L/64$. In the first topology, 9a, for $\alpha = 10^{-4}$, the optimizer failed to remove material, resulting in the termination of the optimization after a specified number of iterations without significant changes in the design. Due to the unmet final volume fraction target of 50%, this instance delivers a resulting relative compliance value of 0.8994, the lowest among the presented cases. This example indicates that for relatively high values of α, the solution does not converge, implying the potential need for a more non-linear filter approach in such scenarios. Using relatively high values for α results in significant geometric differences between the open and close designs. This leads to discrepancies between the computed sensitivities and a build-up of checkerboard patterns. The latter prevents the material from being removed as the optimizer is trapped in a loop of oscillating checkerboard patterns. In Figs. 9b, 9c, and 9d, the volume constraint is satisfied, and the optimized designs have evolved to different local minima. Quantitatively, the most favorable outcome is presented in Fig. 9b with relative compliance of 2.5247. The designs vary in the number of branches and the locations of the bifurcations. Given that the parameter α controls the non-linearity of the filter and directly affects the sensitivities, a change in the final design for each case was anticipated.

Moreover, Fig. 10 shows how the non-linearity parameter affects the final geometry in the case of different volume constraints. Namely, we display the final designs using $\alpha = 10^{-6}$ on the first row and $\alpha = 10^{-8}$ on the second row, subject to volume constraint (from left to right) of 30%, 50%, and 70%, respectively. Here, for both values of α we achieve feasible designs which satisfy the prescribed volume constraints. As noted for Fig. 9, the diverse final designs originate from the optimizer reaching various local minima for different values of α.

5.2 Minimum structural compliance

The second example considers a structural case. Due to the symmetric nature of the problem, only the top half of the domain is resolved in the computations to optimize computational efficiency and time.

The results obtained for varying filter radius sizes are depicted in Fig. 11. The value of RelObj below each optimized design indicates the corresponding relative objective function value, which is attained by dividing the optimized beam's compliance $c_{\text{structural}}$ by the compliance of the solution of the variable thickness sheet problem. Across all cases, the size of the smallest structural member is no smaller than the size of the applied filter. This is indicative of the efficacy of the filter in enforcing length control during

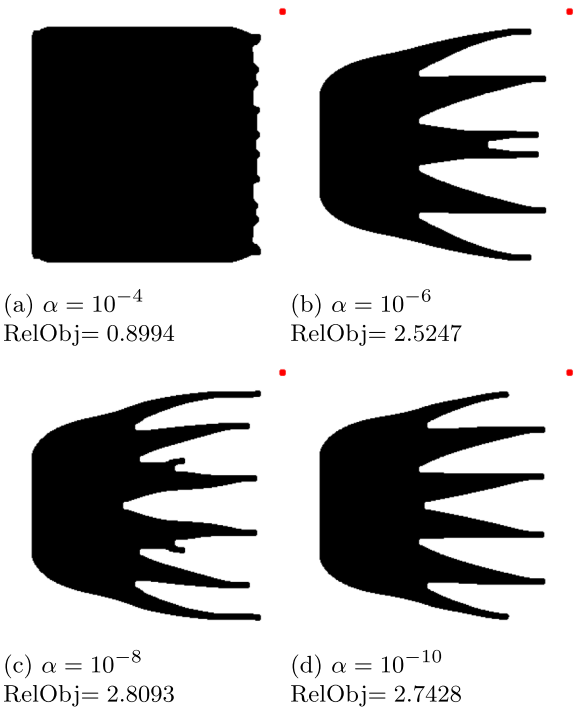

Fig. 9 Optimized designs corresponding to different values of the non-linearity parameter for the minimum thermal compliance problem using a filter radius of $r = L/64$

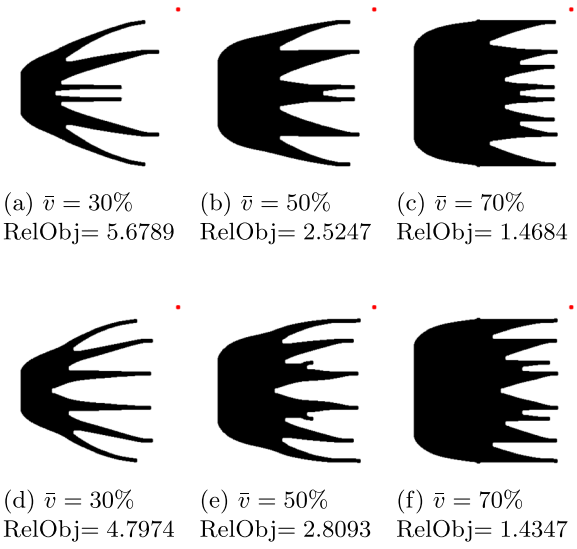

Fig. 10 Optimized structures for different volume constraints and α values. Here, we fix the filter radius to $r = L/64$ and we use $\alpha = 10^{-6}$ on the top row and $\alpha = 10^{-8}$ on the bottom row

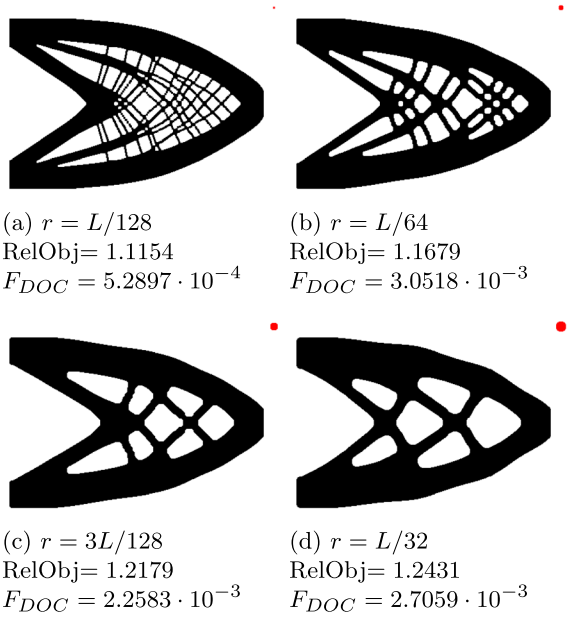

(a) $r = L/128$
RelObj= 1.1154
$F_{DOC} = 5.2897 \cdot 10^{-4}$

(b) $r = L/64$
RelObj= 1.1679
$F_{DOC} = 3.0518 \cdot 10^{-3}$

(c) $r = 3L/128$
RelObj= 1.2179
$F_{DOC} = 2.2583 \cdot 10^{-3}$

(d) $r = L/32$
RelObj= 1.2431
$F_{DOC} = 2.7059 \cdot 10^{-3}$

Fig. 11 Resulting designs for the structural problem with varying filter radius r and relative compliance values. A red circle next to each topology indicates the filter radius size

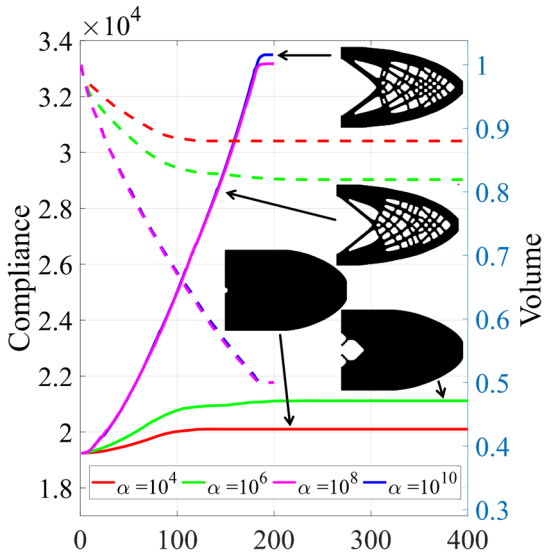

Fig. 12 Evolution of compliance (solid lines) and volume fraction (dashed lines) for four distinct values of the α parameter. The optimized design for each α value is displayed next to the corresponding curve

the topology optimization process. The red region (the discrete circle) next to each design depicts the shape and size of the used filter kernel.

As observed, the elements conform to the minimum size requirements, and the connections between the bars are composed of more than one element, ensuring structural integrity and adherence to the predefined size constraints. With a filter radius of $r = L/64$, in Fig. 11b, the resulting topology of the cantilever beam showcases a unique distribution of material. The central region of the structure is populated with numerous bars, all adhering to the minimum size constraints, while thicker bars are found in the upper and lower regions of the design, possibly due to the increased load-bearing requirements in these areas. This distribution of material indicates that the transition in structural behavior is taken into account by the proposed method as the filter radius increases. Increasing the filter radius to $r = 3L/128$, see Fig. 11c, brings about a more pronounced disparity in material distribution. The bars in the central region become significantly thicker compared to the last result. This results in a structure that has reinforced regions where material is more concentrated. Further increasing the filter radius to $r = L/32$, the observed trends continue. The bars located in the upper and lower regions of the cantilever beam retain more material and exhibit increased thickness, while the central region has thinner structural members. This distribution highlights the influence of the filter radius on the material layout, as larger values of r lead to a more pronounced differentiation in bar thickness across the structure.

The absence of checkerboarding in these cases reaffirms the proposed method's capability to ensure length scale control and achieve stable and reliable designs. The compliance values for each scenario are also presented. A discernible trend is observed in the data: as the filter radius r increases, the compliance increases. This phenomenon can be attributed to that increasing the filter size r decreases the design freedom and thus limits the optimization algorithm's ability to find less compliant structures.

Figure 12 illustrates the evolution of compliance and volume fraction for four separate α parameter settings: 10^{-4}, 10^{-6}, 10^{-8} and 10^{-10}, each subjected to a radius constraint $r = L/64$. Compliance is represented by solid lines, with dashed lines showing the volume fraction's progression over iterative steps. Adjacent to each of the curves, the optimized design for the corresponding α value is exhibited. For α values of 10^{-4} and 10^{-6}, the optimization process ends without fulfilling the volume constraint, as evidenced by the premature stabilization of the volume fraction curve. For relatively high values of α, we get significant geometric differences between the open and close designs, leading to discrepancies between the computed sensitivities. The latter results in a build-up of checkerboard patterns which prevents the material from being removed as the optimizer is trapped in a loop of oscillating checkerboard patterns. Conversely, for α values of 10^{-8} and 10^{-10}, the volume constraint is satisfied, leading to distinct local minima with compliance values that are relatively close. The results underscore the necessity of employing smaller values of the parameter α to achieve convergence.

The approach employed in this work avoids the necessity for continuation in α and penalization parameters. This characteristic offers a possible benefit by simplifying the optimization process, as it eliminates the need for iterative fine-tuning of filter parameters that is usually necessary to achieve convergence. The parameter α thus serves as a singular control variable, directly modulating the filter's non-linearity.

Finally, it is noteworthy that in all results shown in this work, only a limited number of elements transitioned from void to solid states. This characteristic of the results can be primarily attributed to the use of SIMP interpolation. The sensitivity in the void region is effectively zero due to the choice of using SIMP, which does not explicitly account for transitions between void and solid states. Nonetheless, the solutions attained conform remarkably to the imposed length scale requirements, underscoring the efficacy of the method in preserving the design's structural integrity. The transition from void to solid using the proposed filter with TOBS is a future topic of research.

6 Conclusion

This paper presents a filtering scheme that provides length scale control in binary topology optimization. While this is only the third work on the topic, it is the first to provide mathematical guarantees on length scale control. The chosen method was the TOBS. Numerical results showed that, for thermal compliance minimization, the proposed filtering scheme is able to enforce the size of solid regions. Of course, a trade-off between the filter radius and the final objective function is observed. An important observation is that binary design variables appear to reduce the influence of filter parameters compared to their application in continuous methods. This characteristic simplifies the optimization process by reducing the need for extensive parameter tuning, although the results did not converge for all α values. The structural compliance problem was also explored. It is important to mention that, in both (heat and structural) compliance scenarios, the number of flips from void to solid happened in much lower quantities than in the inverse form. Nevertheless, numerical results showed good agreement with the imposed length scale. We expect that the proposed filtering can expand the capabilities of the binary or SAIP-based topology optimization methods and open up new types of applications. Future research can focus on increasing the number of flips from void to solid and applying the length scale filter in other multiphysics problems.

6.1 Integration in Our Work and Applicability

In our research, we tackle the thermal and structural compliance problems using the TOBS method and introduce a length scale control filter. This enhances the current capabilities of binary topology optimization methods. The heuristic is designed to promote control of the minimum size of both solid and void regions. This is especially relevant in the context of additive manufacturing, like 3D printing, where a structure's smallest feature is often limited by the printer's resolution. By integrating this consideration into our optimization process, we ensure that the resulting designs are not only optimized in terms of compliance but possibly with enhanced manufacturability (depending on the filter radius). The aspects of this work effectively bridge the gap between theoretical optimization and length scale control in binary methods. We hope it brings a different perspective to binary methods by ensuring that the optimized designs are not only theoretically sound but also practical for applications that require length scale control.

7 Open Access

Author contributions Conceptualization: Rômulo Cortez, Mario Setta, Renato Picelli, Eddie Wadbro; Methodology and Software: Rômulo Cortez, Mario Setta, Renato Picelli, Eddie Wadbro; Writing - Original Draft: Rômulo Cortez, Mario Setta, Renato Picelli, Eddie Wadbro; Writing - Review and Editing: Rômulo Cortez, Mario Setta, Renato Picelli, Eddie Wadbro; Visualization: Rômulo Cortez, Mario Setta; Funding acquisition: Renato Picelli, Eddie Wadbro.

Funding Open access funding provided by Karlstad University. Renato Picelli thanks the support of the São Paulo Research Foundation (FAPESP) under the grant 2022/13175-2. All the authors thank the support of the Swedish Foundation for International Cooperation in Research and Higher Education (STINT) under the grant IB2022-9471. Eddie Wadbro thanks for the support from the Swedish Research Council under the grant 2022-03783.

Code availability The code is available from the correspondingauthor upon reasonable request.

Declarations

Conflict of interest The authors declare that they have no known competing financial interests or personal relationships that could have appeared to influence the work reported in this paper.

Replication of results All the details necessary to reproduce the results have been defined in the paper.

References

Alonso DH, Romero Saenz JS, Picelli R et al (2022) Topology optimization method based on the wray-agarwal turbulence model. Struct Multidisc Optim 65(3):82

Beckers M (1999) Topology optimization using a dual method with discrete variables. Struct Multidisc Optim 17:14–24

Bendsøe MP, Sigmund O (2003) Topology optimization - theory. Methods and applications. Springer Verlag, Berlin

Guest JK (2009) Topology optimization with multiple phase projection. Comput Methods Appl Mech Eng 199(1–4):123–135

Guest JK, PrÈvost JH, Belytschko T (2004) Achieving minimum length scale in topology optimization using nodal design variables. Int J Num Methods Eng 61(2):238–254

Guest JK, Asadpoure A, Ha SH (2011) Eliminating beta-continuation from heaviside projection and density filter algorihms. Struct Multidisc Optim 44(4):443–453

Hägg L, Wadbro E (2018) On minimum length scale control in density based topology optimization. Struct Multidisc Optim 58:1015–1032

Huang X, Xie YM (2007) Convergent and mesh-independent solutions for the bi-directional evolutionary structural optimization method. Finite Elem Anal Des 43:1039–1049

Hägg L, Wadbro E (2017) Nonlinear filters in topology optimization: existence of solutions and efficient implementation for minimum compliance problems. Struct Multidisc Optim 55:1017–1028. https://doi.org/10.1007/s00158-016-1553-8

Hägg L, Wadbro E (2018) On minimum length scale control in density based topology optimization. Struct Multidisc Optim 58:1015–1032. https://doi.org/10.1007/s00158-018-1944-0

Koga AA, Lopes ECC, Nova HFV et al (2013) Development of heat sink device by using topology optimization. Int J Heat Mass Transf 64:759–772

Lai Y, Li Y, Liu Y et al (2024) Application of bi-directional evolutionary structural optimization to the design of an innovative pedestrian bridge. AI Civil Eng 3:9

Lazarov BS, Wang F, Sigmund O (2016) Length scale and manufacturability in density-based topology optimization. Arch Appl Mech 86:189–218

Liang Y, Cheng G (2019) Topology optimization via sequential integer programming and canonical relaxation algorithm. Comput Methods Appl Mech Eng 348:64–96. https://doi.org/10.1016/j.cma.2018.10.050

Liang Y, Cheng G (2020) Further elaborations on topology optimization via sequential integer programming and canonical relaxation algorithm and 128-line matlab code. Struct Multidisc Optim 61:411–431

Matheron G, Serra J (2001) The birth of mathematical morphology. International Symposium on Mathematical Morphology

Picelli R, Ranjbarzadeh S, Sivapuram R et al (2020) Topology optimization of binary structures under design-dependent fluid-structure interaction loads. Struct Multidisc Optim 62:2101–2116

Picelli R, Sivapuram R, Xie YM (2020) A 101-line MATLAB code for topology optimization using binary variables and integer programming. Struct Multidisc Optim 63(2):935–954

Qiu W, Jin S, Xia L et al (2022) Length scale control schemes for bi-directional evolutionary structural optimization method. Int J Num Methods Eng 123(3):755–773

Sigmund O (2007) Morphology-based black and white filters for topology optimization. Struct Multidisc Optim 33(4–5):401–424

Sivapuram R, Picelli R (2018) Topology optimization of binary structures using integer linear programming. Finite Elem Anal Des 139:49–61

Sun K, Cheng G, Zhang K et al (2024) Sequential conservative integer programming method for multi-constrained discrete variable structure topology optimization. Acta Mechanica Sinica 40(1):423151

Svanberg K, Svärd H (2013) Density filters for topology optimization based on the pythagorean means. Struct Multidisc Optim 48:859–875. https://doi.org/10.1007/s00158-013-0938-1

Svanberg K, Werne M (2006) Topology optimization by sequential integer linear programming. Springer, Dordrecht

Wadbro E, Berggren M (2006) Topology optimization of an acoustic horn. Comput Methods Appl Mech Eng 196(1–3):420–436

Wadbro E, Hägg L (2015) On quasi-arithmetic mean based filters and their fast evaluation for large-scale topology optimization. Struct Multidisc Optim 52:879–888. https://doi.org/10.1007/s00158-015-1273-5

Xia L, Xia Q, Huang X et al (2018) Bi-directional evolutionary structural optimization on advanced structures and materials: a comprehensive review. Arch Comput Methods Eng 25:437–478

Xie YM, Steven GP (1993) A simple evolutionary procedure for structural optimization. Comput Struct 49:885–896

Xu T, Lin X, Xie YM (2023) Bi-directional evolutionary structural optimization with buckling constraints. Struct Multidisc Optim 66(4):67

Yoon GH, Kim YY (2005) The element connectivity parameterization formulation for the topology design optimization of multiphysics systems. Int J Num Methods Eng 64:1649–1677

Zhao ZL, Zhou S, Feng XQ et al (2018) On the internal architecture of emergent plants. J Mech Phys Solids 119:224–239